Structure-property-performance relationship of a series of CO2RR-active N-doped mesoporous carbon frameworks

Jialang Li[a], Ahmed Ali[a,b], Linke Huang[c], Ruohong Sui[a], Robert Marriott[a], Chandra Singh[c], and Viola Birss[a]

[a] Department of Chemistry, University of Calgary, Calgary, Alberta T2N 1N4, Canada
[b] Department of Chemistry, Alexandria University, Alexandria (21568), Egypt.
[c] Department of Materials Science and Engineering, University of Toronto, Toronto, Ontario M5S 3E4, Canada

Supplementary Information

Table S1. Summary of Preparation Methods for N-Doped Carbons

Name	Carbon Precursor	Silica template size (nm)	N-doping method	N-doping outcome	Doping type
N-CIC-12	Mesophase pitch	12	NH_3 heat treatment	N-doping was achieved by exposure of CICs to NH_3 at high temperatures; N functionalities then on exposed surfaces only.	Ex-situ N doping
N-CIC-22	Mesophase pitch	22	NH_3 heat treatment	N-doping was achieved by exposure of CICs to NH_3 at high temperatures; N functionalities then on exposed surfaces only.	Ex-situ N doping
N-CIC-85	Mesophase pitch	85	NH_3 heat treatment	N-doping was achieved by exposure of CICs to NH_3 at high temperatures; N functionalities then on exposed surfaces only.	Ex-situ N doping
Polyaniline Derived -22 (AD-22)	Polyaniline	22	Decompose polyaniline	N and C both derived from the thermal decomposition of polyaniline; N is present in both the carbon walls and on surfaces.	In-situ N doping

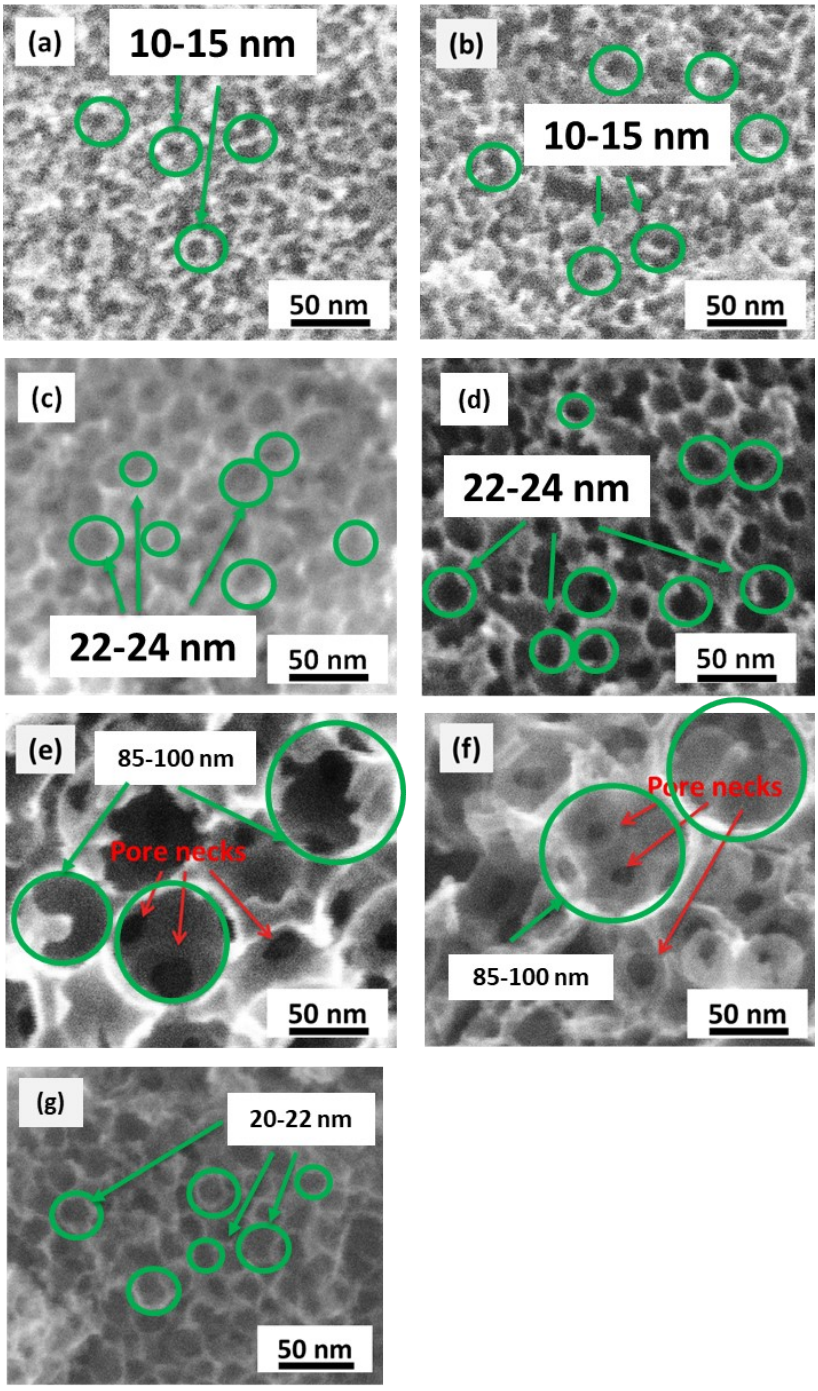

Figure S1. Representative FE-SEM images of (a) CIC-12, (b) N-doped CIC-12, (c) CIC-22, (d) N-doped CIC-22, (e) CIC-85, (f) N-doped CIC-85, and (g) aniline-derived (AD)-22, with the green circles indicating the pores, the numbers giving the pore size, and red arrow.

Table S2. Structural properties of all samples obtained from SEM, gas sorption and electrochemistry

Sample	Pore Size (nm) [a]	S_{BET} [m^2 g^{-1}] [b]	S_{meso} [m^2 g^{-1}] [c]	S_{micro} [m^2 g^{-1}] [d]	S_{micro}/S_{BET} [%]	ECSA [m^2 g^{-1}] [e]
CIC-12	10-15	442 ± 8	380	69	15	452 ± 3
N-CIC-12	10-15	550 ± 24	387	139	26	518 ± 7
CIC-22	22-24	262	221	41	16	217
N-CIC-22	22-24	295	230	64	21	295
CIC-85	85-100	205	179	26	13	195 ± 1
N-CIC-85	85-100	406 ± 21	251 ± 10	155 ± 11	38	401 ± 37
AD-22	20-22	307 ± 13	259 ± 6	48 ± 9	15	281 ± 3

[a] Pore sizes obtained by averaging the width of more than 100 pores in the FE-SEM images.
[b] S_{BET} = Total surface area, obtained using the Brunauer-Emmett-Teller (BET) plot in the partial pressure range of $0.05 < P/P_o < 0.30$.
[c] S_{meso} = Mesoporous surface area and V_{micro} = micropore volume, both obtained using the t-plot method in the partial pressure range of $0.2 < P/P_o < 0.5$, with carbon black used as the reference.
[d] S_{micro} = Micropore surface area, obtained by subtracting the mesoporous surface area (S_{meso}) from the total surface area ($_{SBET}$).
[e] ECSA (m^2 g^{-1}) was obtained by dividing the C_{dl} obtained from Figure S8 by 15 μF cm^{-2}, determined by others for activated carbon microbeads and carbon fibers and both prior electrochemical and gas sorption studies with our group.[1,2] Measurements were repeated 3 times to obtain the error bars.

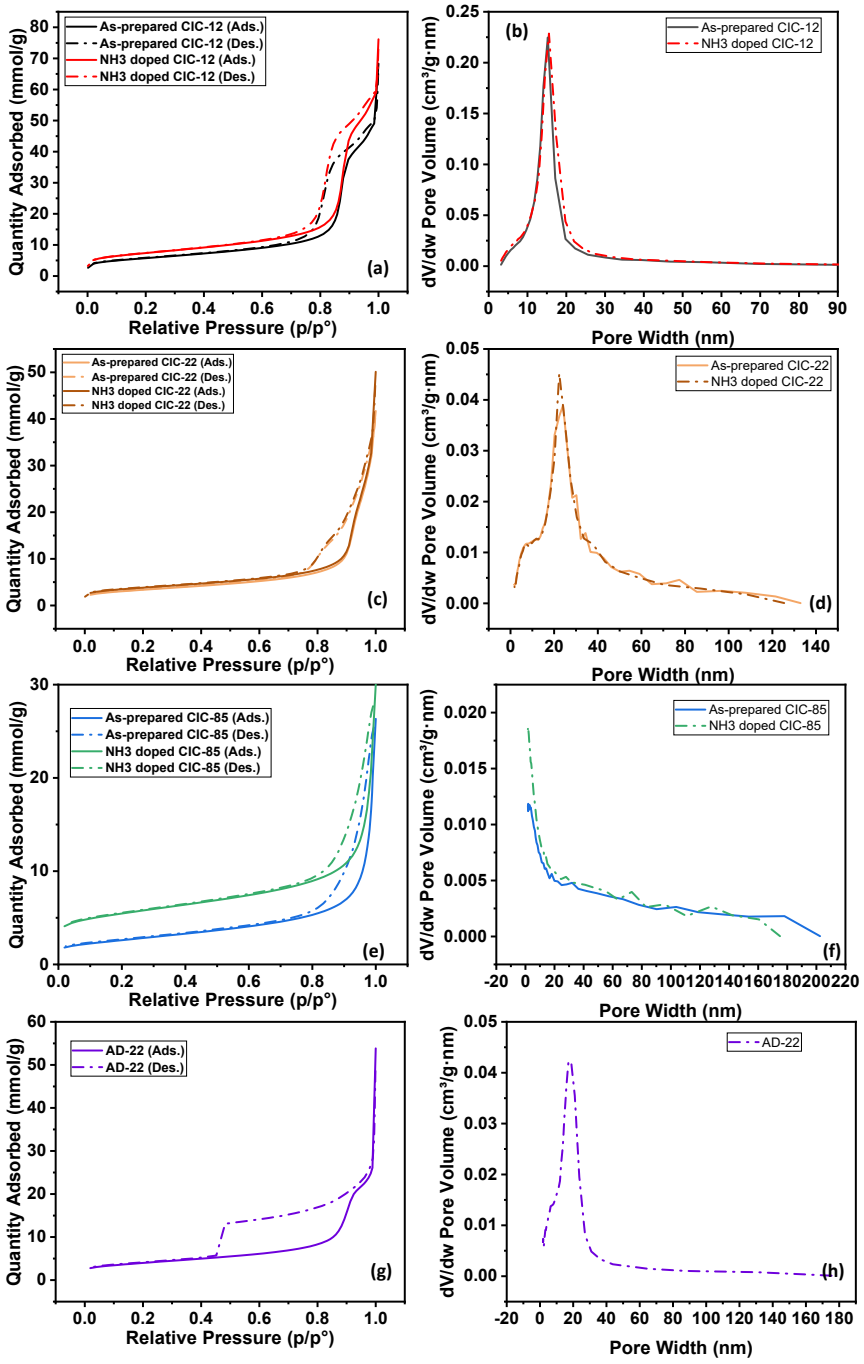

Figure S2. N_2 sorption data of mesoporous carbons with/without N-doping. N_2 adsorption (solid line) and desorption (dashed line) data for both the as-prepared CIC-12, 22 and 85 material, N-doped CIC-12, 22 and 85 material and AD-22. (b, d, f and h) show the corresponding pore size distributions of the materials, calculated from the adsorption branches of the isotherm using the Barrett-Joyner-Halenda (BJH) method The t-curve of Carbon Black was used as the standard for the determination of the statistical thickness of the adsorbed nitrogen film.

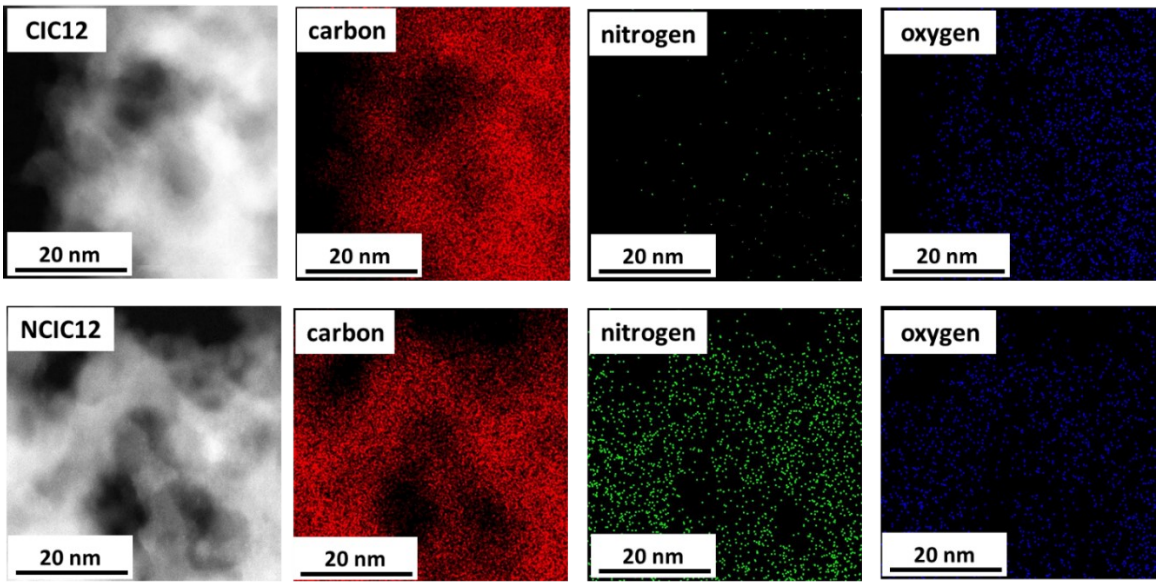

Figure S3. Representative STEM and EDS maps of (top) CIC-12 and (bottom) N-CIC-12. Red dots: carbon; green dots: nitrogen; blue dots: oxygen**.**

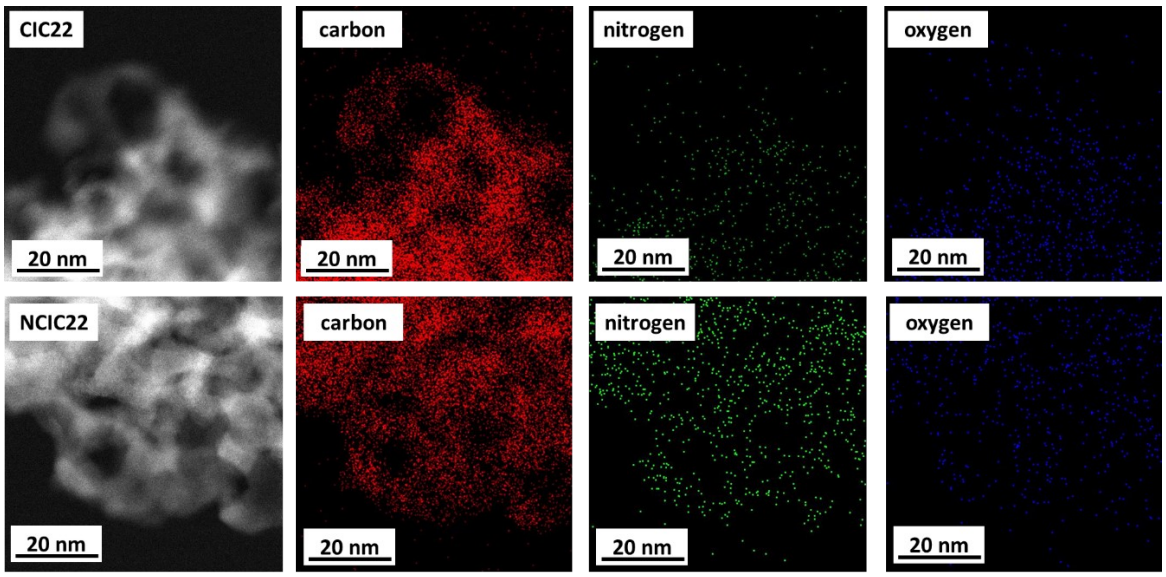

Figure S4. Representative STEM and EDS maps of N-CIC-22. Red dots: carbon; green dots: nitrogen; blue dots: oxygen.

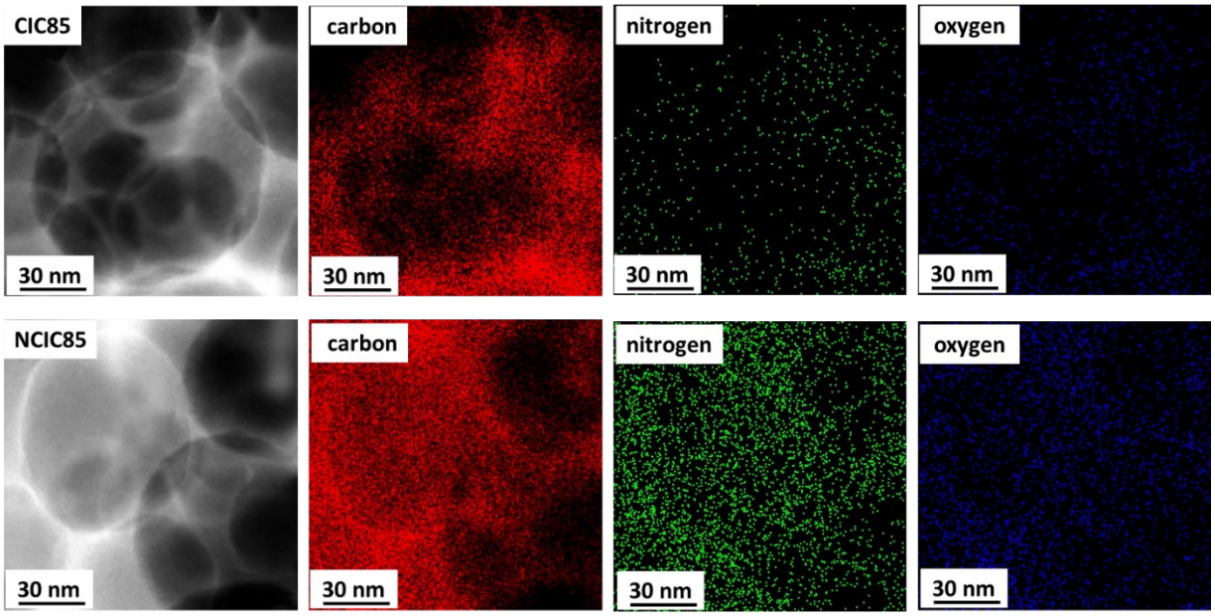

Figure S5. Representative STEM and EDS maps of (top) CIC-85 and (bottom) N-CIC-85. Red dots: carbon; green dost: nitrogen; blue dots: oxygen.

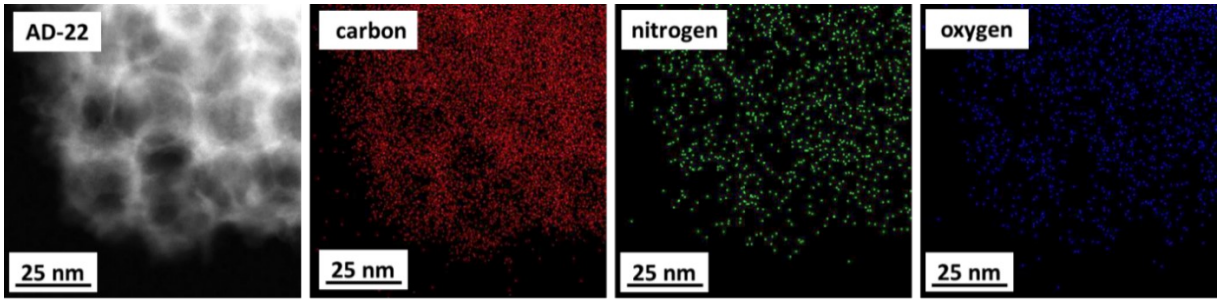

Figure S6. Representative STEM and EDS maps of AD-22. Red dots: carbon; green dots: nitrogen; blue dots: oxygen.

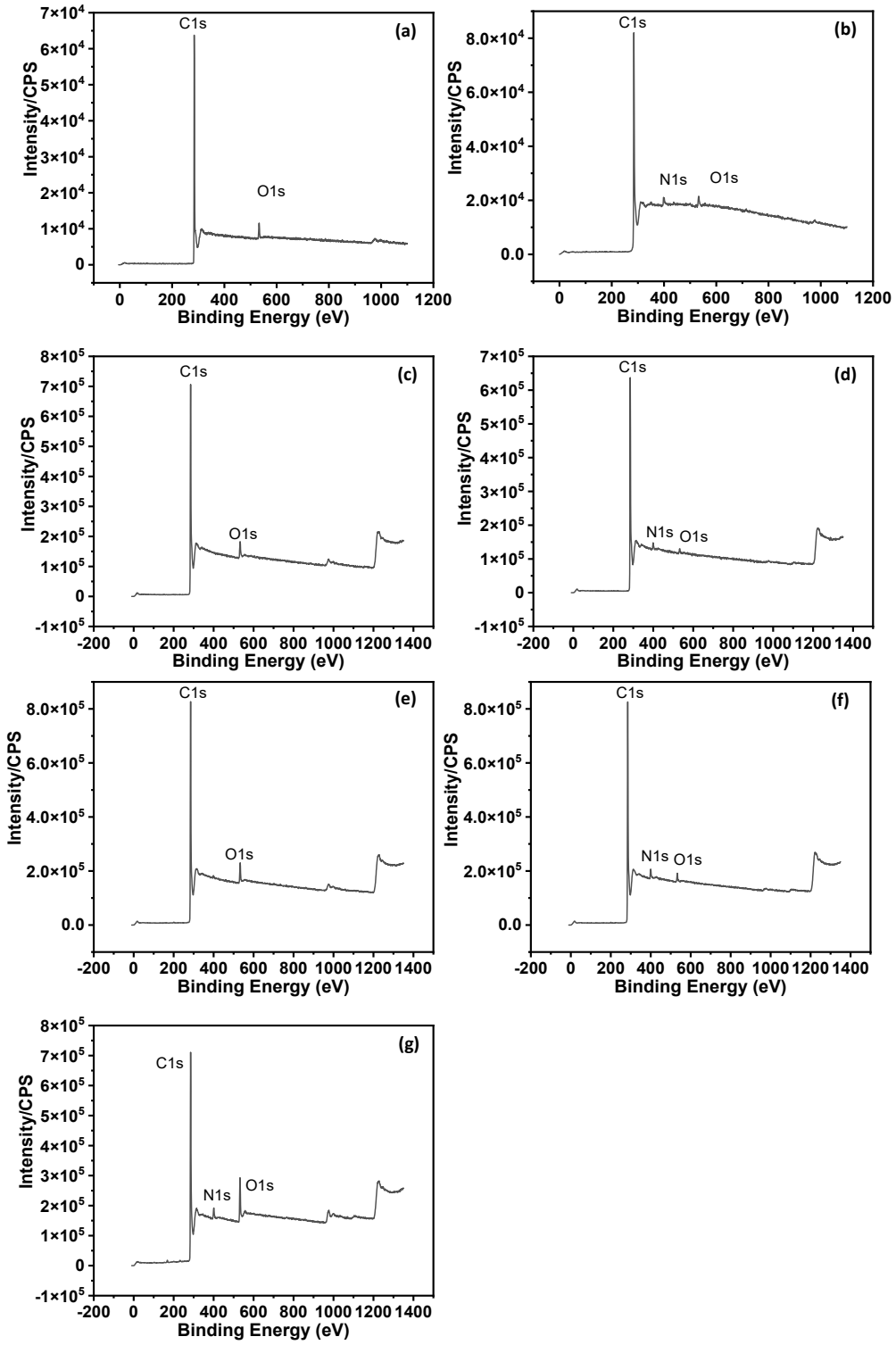

Figure S7. XPS survey scans of the N 1s region for (a) CIC-12, (b) N-CIC-12, (c) CIC-22, (d) N-CIC-22, (e) CIC-85, (f) N-CIC-85, and (g) AD-22.

Table S3. Summary of elemental content (at%) and N speciation of N-doped carbons obtained from XPS analysis

Carbon-based material	C (at %)	N (at %)	O (at %)	N distribution		
				Pyridinic N (%)	Pyrrolic N (%)	Graphitic N (%)
CIC-12	97 ± 4	0	3 ± 0.2	0	0	0
N-CIC-12	93 ± 4	2.3 ± 0.1	5 ± 0.3	53 ± 2	39 ± 2	8 ± 0.4
CIC-22	97 ± 4	0	3 ± 0.2	0	0	0
N-CIC-22	97 ± 4	1.8 ± 0.1	1.2 ± 0.1	43 ± 2	48 ± 2	9 ± 0.4
CIC-85	96 ± 4	0	4 ± 0.2	0	0	0
N-CIC-85	96 ± 4	2.5 ± 0.1	1.4 ± 0.1	37 ± 2	45 ± 2	17 ± 0.8
AD-22	72 ± 4	5 ± 0.2	23 ± 1.2	0	0	100 ± 5

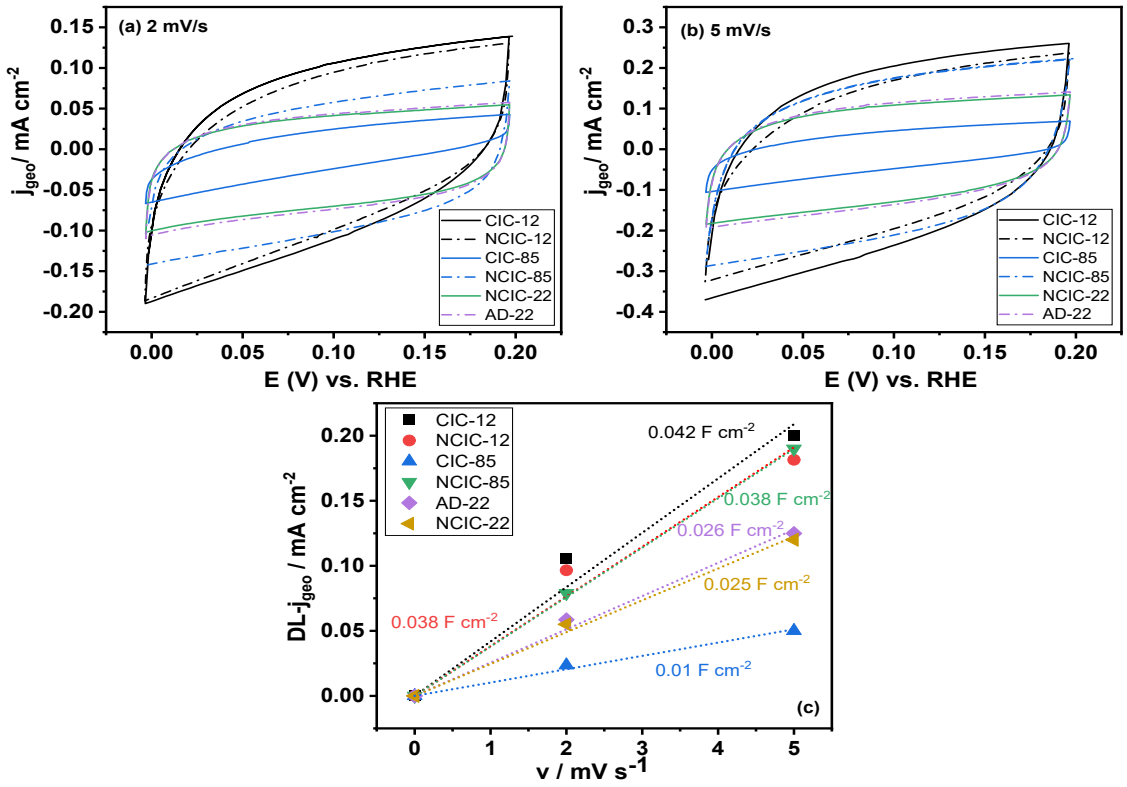

Figure S8. (a,b) Cyclic voltammetry of CIC-12/22/85 before and after N-doping, conducted in CO_2-saturated 0.5 M $KHCO_3$ at various scan rates to determine the double layer (DL) capacitance. **(c)** Current densities from (a,b) plotted vs. scan rate to extract the double layer capacitance, with the slopes obtained by linearly fitting the value of (ja-jc)/2 at 0.1 V vs. RHE vs. scan rate. All CVs were collected between 0.0 and 0.2 V vs. RHE to avoid interference from Faradaic processes such as the HER (at negative of 0 V vs. RHE), CO_2RR (negative of -0.11 V vs. RHE) and detectable carbon oxidation or irreversible oxidation to form trace amounts of CO_2 (above ca. 0.9 V vs. RHE).[3]

Table S4 – Summary of N-C sources/properties and CO_2RR performance in bicarbonate solutions in H-cell experiments from the literature

Catalyst	Preparation method	Onset over-potential (V)	Max FE (%)	E vs. RHE @ Max FE (V)	i_{CO} @ Max FE ($mA\ cm^{-2}$)	N at. %	BET ($m^2\ g^{-1}$)	Lit. ref #
NDC-700	Heat treated under N_2	-0.35	84	-0.82	6.6	3.6	1269	[4]
CNPC	NH_3 etching	-0.39	92	-0.60	0.30	3.9	974	[5]
MNC-D	DMF treatment	-0.19	92	-0.58	6.8	17	732	[6]
WNCN	NH_3 etching	-0.19	84	-0.60	1.2	4.3	812	[7]
3D-NG	CVD	-0.19	85	-0.58	1.5	6.6	-	[8]
NPC-1000	MOF calcination	-0.24	98	-0.55	3.0	2.1	-	[9]
NC-900-HH	NH_3 etching	-0.19	90	-0.50	0.40	3.7	1530	[10]
NR/CS-900	Activation ($ZnCl_2$) and pyrolysis	-0.10	94	-0.45	0.94	5.3	860	[11]
NCNT	CVD	-0.18	80	-0.8	1.5	5.0	-	[12]
NCNT-3-700	Pyrolysis	-0.29	90	-0.90	5.4	1.8	327	[13]
NPC-900	Activation (KOH)/Pyrolysis	-0.16	95	-0.67	2.3	1.9	545	[14]
N-CWM	Pyrolysis	-0.31	78	-0.68	1.6	5.5	877	[15]
NCB3	Heat treated under N2	-0.30	64	-0.70	1.5	5.3	603	[16]
Mf-NC-1000	Heat treated under Ar, then HF etching	-0.30	90	-0.55	0.90	-	-	[17]
N-C 700	Heat treated under N_2	-0.40	94	-1.20	5.4	5.6	410	[18]
NC800	Heat treated under N_2	-0.45	97	-0.86	9.1	4.5	890	[19]
CB-NGC-2	Heat treated under Ar	-0.26	91	-0.56	3.7	5.4	1673	[20]
NDAPC	NH3-etching	-0.50	83	-0.90	3..8	4.2	459	[21]
N-CIC-12	NH_3 etching	-0.24	100	-0.45	0.52	2.3	550	**This Work**
N-CIC-22	NH_3 etching	-0.34	20	-0.75	0.10	1.8	295	
N-CIC-85	NH_3 etching	-0.25	48	-0.55	0.30	2.5	406	

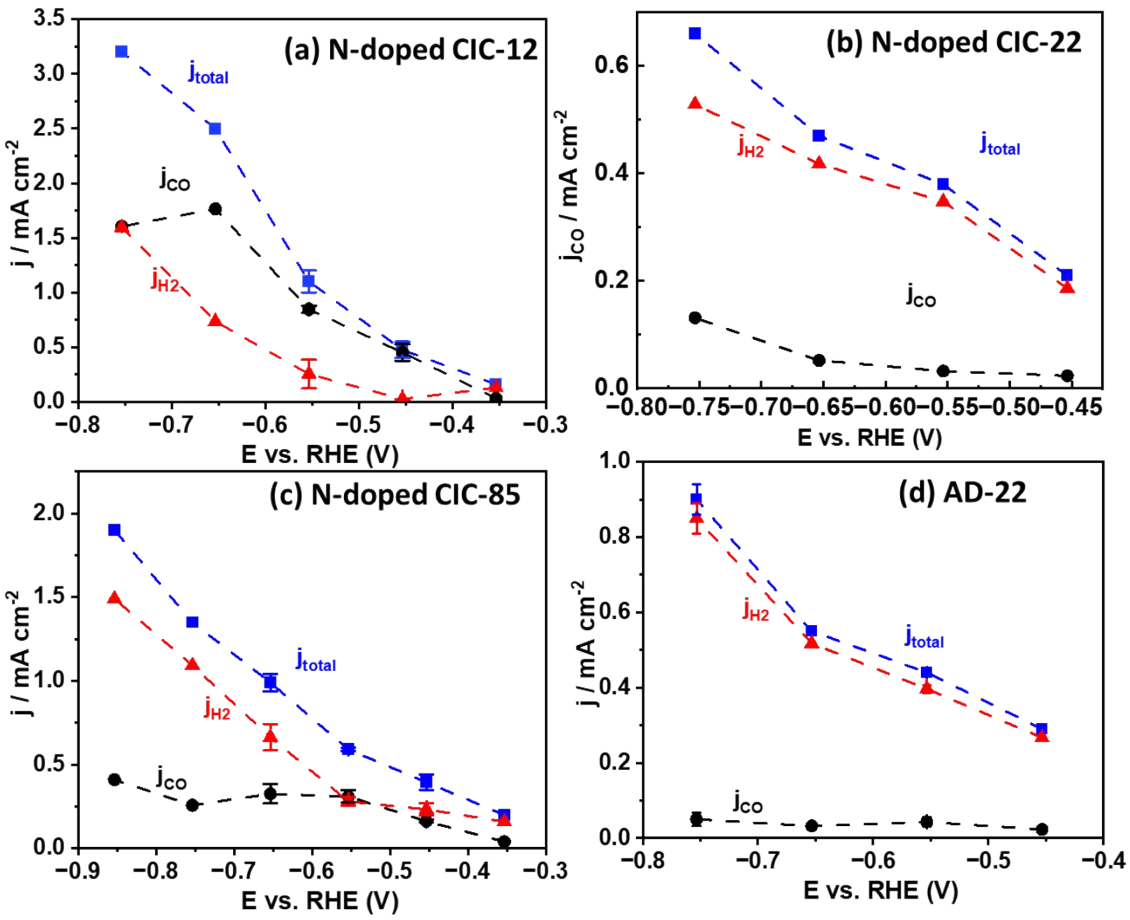

Figure S9. Measured current densities obtained from the N-doped carbon materials in chronoamperometry experiments after roughly 200 seconds at constant potentials for (a) N-CIC-12, (b) N-CIC-22, (c) N-CIC-85, and (d) AD-22.

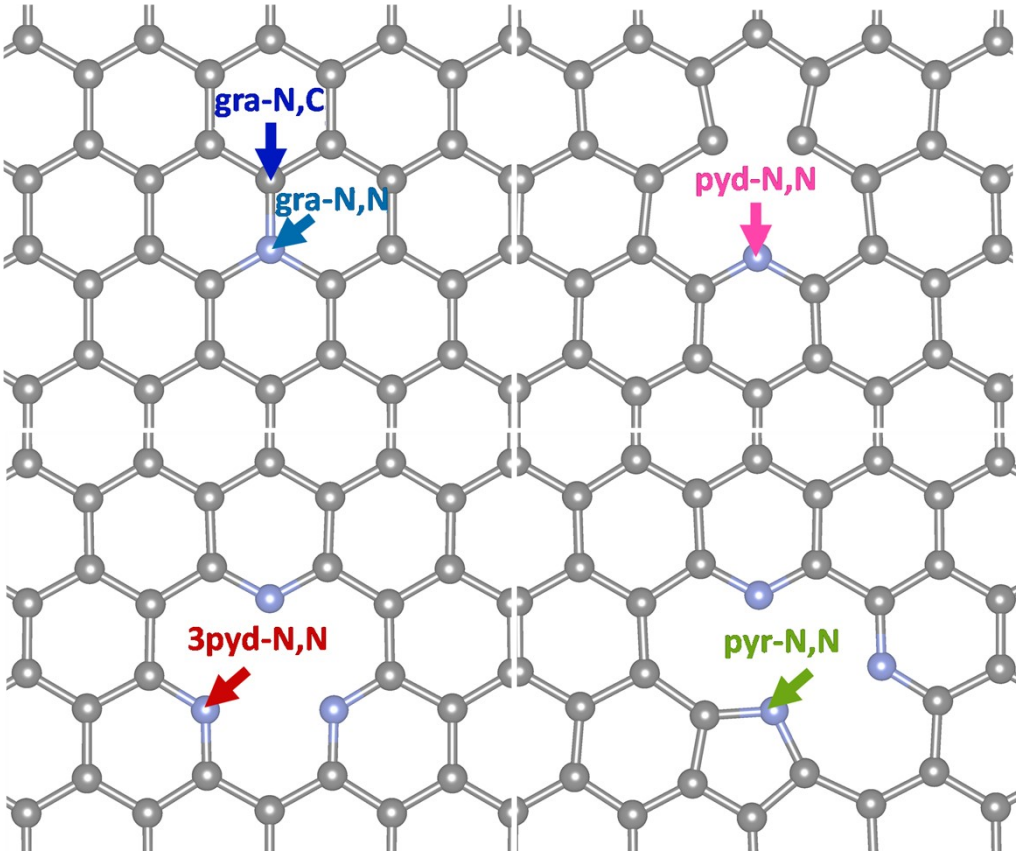

Figure S10. Schematic illustration of N-doped site (blue atoms) configurations on defective graphene surfaces, showing: (top-left, blue and turquoise) graphitic-N,C and graphitic-N,N, respectively; (top-right, pink) pyridinic-N; (bottom-left, red) triple-pyridinic-N; and (bottom-right, green) pyrrolic-N.

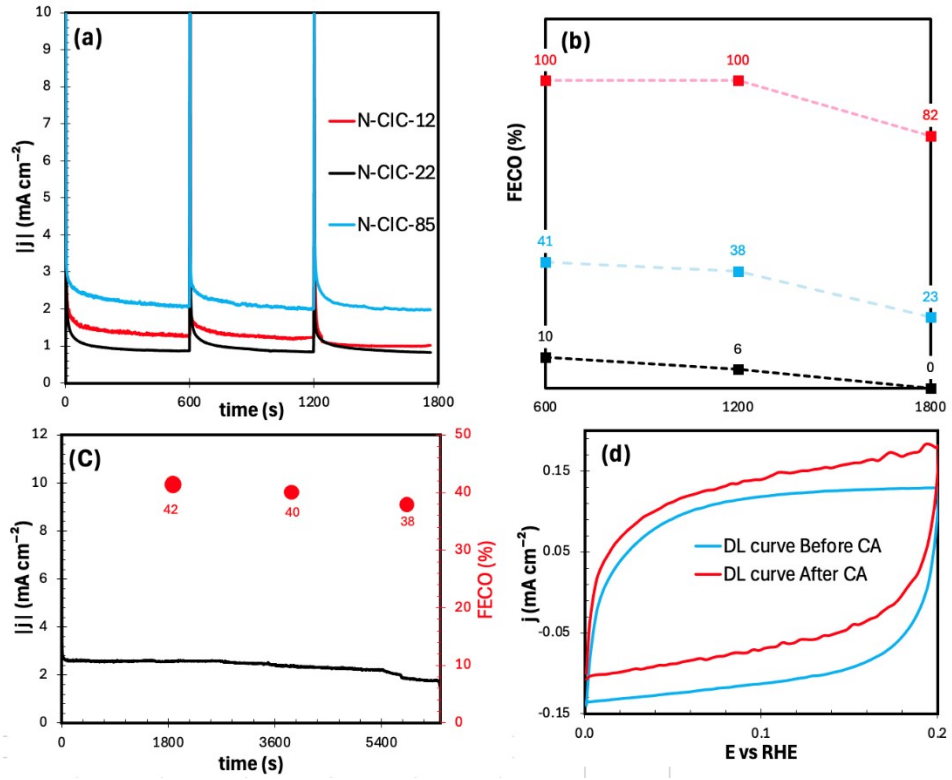

Figure S11. Stability evaluation of CO_2RR at N-doped CIC catalysts in CO_2-saturated 0.5 M $KHCO_3$. **(a)** Chronoamperometry during repeated 10 min polarization cycles at potentials corresponding to the maximum FE_{CO} values for N-CIC-12 (–0.45 V), N-CIC-22 (–0.45 V), and N-CIC-85 (–0.55 V vs. RHE), deposited on carbon paper at a loading of 0.4 mg cm^{-2}. Vertical spikes indicate the times at which the electrolysis was paused, and gas samples were collected for CO analysis. **(b)** Corresponding FE_{CO} values determined by GC analysis of the headspace gas, collected every 10 min, with a 30 min CO_2 purge between consecutive measurements. **(c)** Longer-term CA stability of the N-CIC-85 catalyst at –0.55 V vs. RHE in CO_2-saturated 0.5 M $KHCO_3$ under continuous CO_2 flow for 6400 s, showing the evolution of current density (black, left axis) and FE_{CO} (red, right axis) over time. **(d)** Cyclic voltammograms (3 mV/s) of the N-CIC-85 cathode, collected in CO_2-saturated 0.5 M $KHCO_3$ before and after long-term CA stability testing within the non-Faradaic potential range, showing a minor loss in active area, consistent with partial dislodgement of some of the N-CIC-85/Nafion catalyst under continuous CO_2 bubbling conditions.

References

1 H. Shi, *Electrochim. Acta*, 1996, **41**, 1633–1639.
2 D. Banham, F. Feng, J. Burt, E. Alsrayheen and V. Birss, *Carbon*, 2010, **48**, 1056–1063.
3 B. Pan, M. O. Valappil, R. Rateick, Jr., C. R. Clarkson, X. Tong, C. Debuhr, A. Ghanizadeh and V. I. Birss, *Chem. Sci.*, 2023, **14**, 1372–1385.
4 F. Li, M. Xue, G. P. Knowles, L. Chen, D. R. MacFarlane and J. Zhang, *Electrochim. Acta*, 2017, **245**, 561–568.
5 C. Li, Y. Wang, N. Xiao, H. Li, Y. Ji, Z. Guo, C. Liu and J. Qiu, *Carbon*, 2019, **151**, 46–52.
6 M. Kuang, A. Guan, Z. Gu, P. Han, L. Qian and G. Zheng, *Nano Res.*, 2019, **12**, 2324–2329.
7 H. Li, N. Xiao, M. Hao, X. Song, Y. Wang, Y. Ji, C. Liu, C. Li, Z. Guo and F. Zhang, *Chem. Eng. J.*, 2018, **351**, 613–621.
8 J. Wu, M. Liu, P. P. Sharma, R. M. Yadav, L. Ma, Y. Yang, X. Zou, X.-D. Zhou, R. Vajtai, B. I. Yakobson, J. Lou and P. M. Ajayan, *Nano Lett.*, 2016, **16**, 466–470.
9 L. Ye, Y. Ying, D. Sun, Z. Zhang, L. Fei, Z. Wen, J. Qiao and H. Huang, *Angew. Chem., Int. Ed.*, 2020, **59**, 3244–3251.
10 P. Yao, Y. Qiu, T. Zhang, P. Su, X. Li and H. Zhang, *ACS Sustain. Chem. Eng.*, 2019, **7**, 5249–5255.
11 Y. Zhu, K. Lv, X. Wang, H. Yang, G. Xiao and Y. Zhu, *J. Mater. Chem. A*, 2019, **7**, 14895–14903.
12 J. Wu, R. M. Yadav, M. Liu, P. P. Sharma, C. S. Tiwary, L. Ma, X. Zou, X.-D. Zhou, B. I. Yakobson, J. Lou and P. M. Ajayan, *ACS Nano*, 2015, **9**, 5364–5371.
13 J. Xu, Y. Kan, R. Huang, B. Zhang, B. Wang, K.-H. Wu, Y. Lin, K. Sun, X. Cheng, D. C. W. Tsang, J. Li and K. M. Thomas, *ChemSusChem*, 2016, **9**, 1085–1089.
14 W. Liu, J. Qi, P. Bai, W. Zhang and L. Xu, *Appl. Catal. B*, 2020, **272**, 118974.
15 H. Zhang, S. Min, F. Wang, Z. Zhang and C. Kong, *New J. Chem.*, 2020, **44**, 6125–6129.
16 G. An, K. Wang, M. Yang, J. Zhang, H. Zhong, L. Wang and H. Guo, *Molecules*, 2025, **30**, 953.
17 C. Liu, Y. Wu, J. Fang, K. Yu, H. Li, W. He and C. Chen, *Chin. J. Catal.*, 2022, **43**, 1697–1702.
18 C. Zhang, T. Liu and B. Lu, *Langmuir*, 2025, **41**, 29400–29411.
19 Q. Zeng, G. Yang, J. Chen, Q. Zhang, Z. Liu, B. Qin and F. Peng, *Carbon*, 2023, **202**, 1–11.
20 X. Hao, X. An, A. M. Patil, P. Wang, X. Ma, X. Du and G. Guan, *ACS Appl. Mater. Interfaces*, 2021, **13**, 3738–3747.
21 H. Ning, D. Guo, X. Wang, Z. Tan, W. Wang, Z. Yang and M. Wu, *J. Energy Chem.*, 2021, **56**, 113–120.